DRUG DEVELOPMENT RESEARCH 74 : 259–271 (2013)

DDR

Research Article

Synthesis and Pharmacological Evaluation of New Pyridazin-Based Thioderivatives as Formyl Peptide Receptor (FPR) Agonists

Letizia Crocetti,[1] Claudia Vergelli,[1] Agostino Cilibrizzi,[1] Alessia Graziano,[1] Andrei I. Khlebnikov,[2] Liliya N. Kirpotina,[3] Igor A. Schepetkin,[3] Mark T. Quinn,[3] and Maria Paola Giovannoni[1]*

[1]*Dipartimento di Scienze Farmaceutiche, Sesto Fiorentino 50019, Firenze, Italy*
[2]*Department of Chemistry, Altai State Technical University, Barnaul, Russia*
[3]*Department of Immunology and Infectious Diseases, Montana State University, Bozeman, Montana 59717, USA*

Strategy, Management and Health Policy				
Enabling Technology, Genomics, Proteomics	Preclinical Research	Preclinical Development Toxicology, Formulation Drug Delivery, Pharmacokinetics	Clinical Development Phases I-III Regulatory, Quality, Manufacturing	Postmarketing Phase IV

ABSTRACT A new series of pyridazinone-based thioderivatives and pyridazine analogs was synthesized and tested for their ability to bind to the three human formyl peptide receptor (FPR) isoforms (FPR1, FPR2, and FPR3) and to activate intracellular calcium mobilization and chemotaxis in human neutrophils. Among the pyridazin-3(2*H*)-one derivatives tested, analogs **8b** and **8c** were mixed FPR1/FPR2 agonists, with median effective concentration values in the micromolar range, and were able to activate chemotaxis and Ca^{2+} flux in human neutrophils in the low micromolar range. Molecular docking studies showed that interaction of a ligand with Arg205 of FPR1 is important for FPR1 agonist activity. For FPR2, differences in activity between oxygen-containing compounds and their thio-analogs were due to steric bulkiness of sulfur-containing groups. Drug Dev Res 74 : 259–271, 2013.

Key words: pyridazine; pyridazin-3(2*H*)-one; formyl peptide receptors; neutrophil; chemotaxis; Ca^{2+} mobilization

INTRODUCTION

Formyl peptide receptors (FPRs) are a family of chemoattractant receptors that play an essential role in host defense against infection and trauma. In addition, they are involved at different levels in the regulation of inflammatory reactions and sensing cellular dysfunction [Migeotte et al., 2006]. FPRs belong to the seven transmembrane domain G-protein-coupled receptor family, are expressed in the majority of white blood cells, and are important in host defense and inflammation [Ye et al., 2009]. All major neutrophil functions accomplished through FPRs can be inhibited by treatment with pertussis toxin [Bokoch and Gilman, 1984], indicating that the G proteins coupled to FPRs belong to the G_i family of heterotrimeric proteins [Simon et al., 1991]. Activation of FPRs induces a variety of responses, e.g. directional movement of neutrophils, lysosomal enzyme release [Schiffmann et al., 1975], degranulation, and production of superoxide anion [Prossnitz and Ye, 1997; Mills et al., 1999; Le et al., 2002]. Three FPR subtypes have been identified in humans (FPR1, FPR2, and FPR3) [Ye et al., 2009]. FPR1 was the first that was biochemically defined and was a high-affinity binding site on the surface of

*Correspondence to: Maria Paola Giovannoni, Dipartimento di Scienze Farmaceutiche, Via Ugo Schiff 6, Sesto Fiorentino 50019, Firenze, Italy.
E-mail: mariapaola.giovannoni@unifi.it

Received 23 January 2013; Accepted 4 February 2013

Published online in Wiley Online Library (wileyonlinelibrary.com). DOI: 10.1002/ddr.21076

neutrophils for the prototypic peptide formyl-methionine-leucine-phenylalanine (fMLF) [Ye et al., 2009]. FPR2 shares 69% amino acid identity with human FPR1, but despite the relatively high level of sequence homology, is a low-affinity receptor for fMLF [Quehenberger et al., 1993]. FPR3 shares 56% and 83% sequence identity with human FPR1 and FPR2, respectively, but does not bind N-formyl peptides, e.g. fMLF. Instead, FPR3 responds to some nonformylated chemotactic peptides identified as FPR2 agonists.

FPRs interact with a wide range of structurally different pro- and anti-inflammatory ligands associated with different diseases, including amyloidosis and Alzheimer's disease [Cui et al., 2002], some types of cancers and related alopecia induced by most anticancer agents [Edwards et al., 2005; Tsuruky et al., 2007], prion diseases [Zhou et al., 2009], HIV [Kilby et al., 1998], stomach ulcers [De Paulis et al., 2004], and nociception associated with inflammatory processes [Pieretti et al., 2004]. Many studies indicate that FPRs are important mediators of key events in endogenous anti-inflammation, and it has been proposed that FPR modulation is an attractive approach for the targeting biochemical processes for resolving inflammation [Gilroy et al., 2004]. Likewise, FPRs may represent therapeutic targets for selectively stimulating innate immune responses [Serhan et al., 2007; Zhang and Falla, 2009; Dufton and Perretti, 2010].

Previous studies led to the identification of a wide range of structurally unrelated nonpeptide and peptide FPR agonists, including synthetic molecules and both host-derived and pathogen-derived agents [Bokoch et al., 1984; Gierschik et al., 1989], and more recently, we identified a large number of potent FPR agonists with a pyridazin-3(2*H*)-one scaffold that contained a methoxybenzyl group at position 4 [Cilibrizzi et al., 2009, 2012]. Two of the most interesting compounds of the series are shown in Figure 1: compound **1** is a mixed FPR1/FPR2 agonist with activity in the low micromolar range (median effective concentration values [EC_{50}] = 3.4 and 3.8 μM for FPR1 and FPR2, respectively), whereas compound **2** is a FPR2-specific agonist (EC_{50} = 2.4 μM). Structural analysis of this series of compounds indicated that an acetamide spacer at *N*-2 of the pyridazinone ring is an essential requirement for specificity and potency of these compounds, and the role of both C = O (H-bond acceptor) and amidic NH (H-bond donor) in the side chain was crucial for binding to FPRs. Moreover, the presence of a lipophilic and/or electronegative *para* substituent in the aromatic system of the side chain at position 2 was an important element required for potency and selectivity [Cilibrizzi et al., 2009].

Based on previous reports demonstrating beneficial substitutions of C = S for C = O and methylthio (SCH_3) for methoxy (OCH_3) [Wrobel et al., 1989; Güngör et al., 2006], we designed a series of thio-analogs characterized by properties similar to those of previously reported parent compounds [Cilibrizzi et al., 2009]. Furthermore, a series of pyridazine analogs where the phenylacetamide moiety was moved to position 3 of the ring was also designed. For all new compounds, we report herein the synthesis and biological evaluation for FPR agonist activity, selectivity versus FPR1/FPR2/FPR3, and the ability to activate intracellular calcium mobilization and chemotaxis in human neutrophils.

MATERIALS AND METHODS

Chemistry

Syntheses of the new pyridazin-3(2*H*)-one and pyridazine thioderivatives are depicted in Figures 2 and 3. In Figure 2, procedures to obtain the pyridazinone-3(2*H*)-one thioderivatives **8a-c**, **9** and the thiopyridazine analog **11** are reported. In both cases, the starting material was the 6-methyl-4,5-dihydropyridazin-3(2*H*)-one compound **4** [Meng and Hesse, 1990], which was directly converted in the new benzyl derivative **5a** and the previously described **5b,c** [Cilibrizzi et al., 2009] by Knoevenagel condensation using the appropriate aromatic aldehyde in the

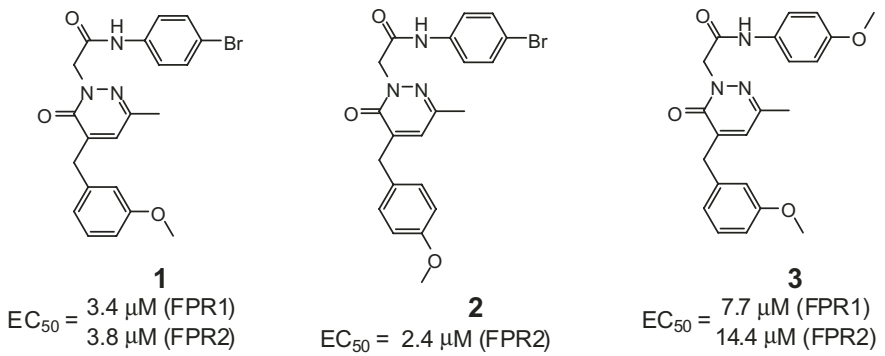

Fig. 1. Structures of selected FPRs agonists **1–3**.

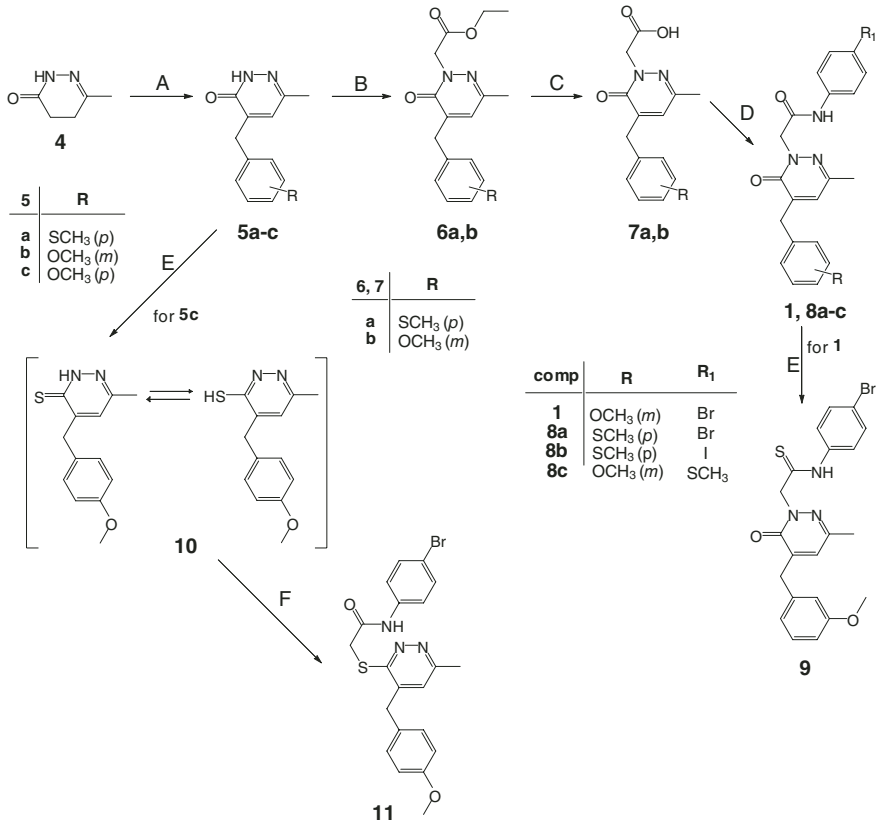

Fig. 2. Synthesis of pyridazin-3(2*H*)-one-based thioderivatives **8a-c**, **9** and pyridazine analog **11**.
Reagents and conditions: (**A**) substituted benzaldehyde (1 equiv), KOH 5% (w/v) in anhydrous EtOH, 1–5 h, reflux; (**B**) ethyl bromoacetate (1.5 equiv), K_2CO_3 (2 equiv), anhydrous CH_3CN, 2–4 h, reflux; (**C**) NaOH 6 N, 1–2 h, 80°C; (**D**) ethyl chloroformate (1.1 equiv), Et_3N (3.5 equiv), substituted aniline (2 equiv), anhydrous THF, 12 h, –5°C → rt; (**E**) Lawesson's reagent (2 equiv), anhydrous toluene, 2–3 h, 80°C; (**F**) *N*-(4-bromophenyl)-2-chloroacetamide (1.5 equiv), K_2CO_3 (2 equiv), anhydrous CH_3CN, 3 h, reflux.

presence of KOH in absolute EtOH (5% w/v). Alkylation of intermediates **5a, 5b** with ethyl bromoacetate resulted in the esters **6a, 6b**, [Cilibrizzi et al., 2009], which after alkaline hydrolysis gave the corresponding acids **7a,b** [Cilibrizzi et al., 2009]. Subsequent reaction of **7a,b** with ethyl chloroformate in THF in presence of triethylamine resulted in the intermediate mixed anhydrides, which in turn were transformed in good yields into the final amide **1** [Cilibrizzi et al., 2009] and the new compounds **8a-c**. Moreover, the thioamide analog **9** was directly generated from compound **1** by treatment with Lawesson's reagent in toluene at 80°C [Jesberger et al., 2003]. Considering that compound **1** has two carbonyl groups susceptible to thionation, both ^{1}H NMR and MS(ESI) analyses were performed to confirm structure **9**. MS analysis clearly demonstrated the presence of a fragment of compound **9** containing the pyridazinone nucleous, and ^{1}H NMR experiments showed a clear difference in the chemical shift of the signal related to N-CH_2-CO in **1** and the corresponding N-CH_2-CS in compound **9**. These findings suggest that the pyridazinone ring was unchanged, and the sulfur was present only and univocally on the side chain. Figure 2 also depicts the synthetic procedure for obtaining the pyridazine analog **11**. Using Lawesson's reagent, as described above, the precursor **5c** [Cilibrizzi et al., 2009] was transformed into the intermediate **10** which, in turn, was alkylated under standard conditions with *N*-(4-bromophenyl)-2-chloroacetamide [Baraldi et al., 2007] to obtain the final compound **11**, containing the phenylacetamide moiety at C-3 of the ring.

The synthetic procedure to obtain pyridazine analogs **15a,b** and **18** is depicted in Figure 3. The previously described 3-chloro-6-phenylpyridazin-4-ol, compound **12** [Sircar, 1983] was converted into intermediate **13** by performing a cross-coupling reaction with the appropriate aryl boronic acids, using copper acetate as catalyst and a weak base (triethylamine) in CH_2Cl_2 [Quach and Batey, 2003; Chiang and Olsson, 2004]. Compound **13** was then treated with saturated ethanolic ammonia at 180°C to obtain the corresponding 3-amino derivative **14**, which was directly reacted under standard conditions with the 4-bromophenylisocyanate or the 4-bromobenzoyl

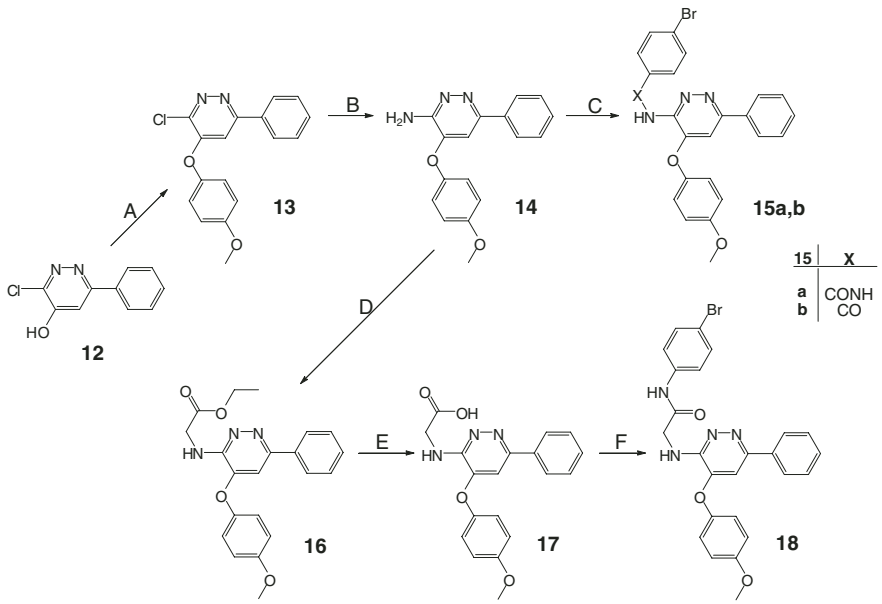

Fig. 3. Synthesis of pyridazine-based analogs **15a**,**b** and **18**.
Reagents and conditions: (**A**) 4-methoxyphenylboronic acid (2 equiv), $Cu(OAc)_2$ (1.5 equiv), Et_3N (2 equiv), CH_2Cl_2, 12 h, rt; (**B**) NH_3/anhydrous EtOH, 7 h, 180°C; (**C**) for **15a**: 4-bromophenylisocyanate (1.1 equiv) anhydrous toluene, 6 h, reflux; for **15b**: 4-bromobenzoyl chloride (4 equiv), Et_3N (catalytic), anhydrous CH_2Cl_2, 24 h, 0°C/rt; (**D**) ethyl bromoacetate (3 equiv), K_2CO_3 (2 equiv), anhydrous CH_3CN, 8 h, reflux; (**E**) NaOH 6 N, 2 h, 80°C; (**F**) ethyl chloroformate (1.1 equiv), Et_3N (3.5 equiv), 4-bromoaniline (2 equiv), anhydrous THF, 12 h, –5°C/rt.

chloride to obtain the urea **15a** and the amide **15b**, respectively. Alternatively, final compound **18** was prepared from intermediate **14** by performing the same reaction sequence (alkylation with ethyl bromoacetate, alkaline hydrolysis, and finally, through the intermediate mixed anhydride, coupling with 4-bromoaniline) shown in Figure 2 for compounds **1** and **8a-c**.

Experimental

All chemicals were purchased from Sigma-Aldrich (St. Louis, MO, USA). Extracts were dried over Na_2SO_4, and the solvents were removed under reduced pressure. All reactions were monitored by thin layer chromatography (TLC) using commercial plates precoated with Merck silica gel 60 F-254 (Merck, Darmstadt, Germany). Visualization was performed by UV fluorescence ($\lambda_{max} = 254$ nm) or by staining with iodine or potassium permanganate. Chromatographic separations were performed on a silica gel column by gravity chromatography (Kieselgel 40, 0.063–0.200 mm; Merck) or flash chromatography (Kieselgel 40, 0.040–0.063 mm; Merck). All melting points were determined on a microscope hot stage Büchi apparatus (Assago, Milano, Italy) and are uncorrected. Yields refer to chromatographically and spectroscopically pure compounds, unless otherwise stated. The identity and purity of intermediates and final compounds were ascertained through ^{1}H NMR and TLC. ^{1}H NMR spectra were recorded with Avance 400 instruments (Bruker Biospin Version 002, Bruker AXS Inc., Madison, WI USA with full digital signal generation [SGU]). Chemical shifts (δ) were reported in ppm to the nearest 0.01 ppm, using the solvent as the internal standard. Coupling constants (J-values) are given in Hz and were calculated using TopSpin 1.3 software (Bruker) rounded to the nearest 0.1 Hz. Mass spectra (m/z) were recorded on an ESI-MS triple quadrupole mass spectrometer (Varian 1200L, Sunnyvale, CA USA). Microanalyses were performed with a Perkin-Elmer 260 elemental analyzer (Waltham, MA USA) for C, H, and N, and the results were within ± 0.4% of the theoretical values, unless otherwise stated.

General procedure for compounds (5a-c)

To 12 ml of a solution of KOH in absolute EtOH (5%, w/v), compound **4** (4.46 mmol) and the appropriate aromatic aldehyde (4.46 mmol) were added, and the solution was refluxed under stirring for 1–5 h. After cooling, the mixture was concentrated *in vacuo*, diluted with ice-cold water (20–25 ml) and acidified with 2 N HCl. The suspension was extracted with CH_2Cl_2 (3×25 ml), and removal of the solvent resulted in compounds **5a-c**, which were purified by crystallization in ethanol.

6-Methyl-4-[4-(methylthio)benzyl]pyridazin-3(2*H*)-one (5a)

Mp = 151–153°C; crystallization solvent = EtOH; yield = 46%. ^{1}H NMR ($CDCl_3$), δ: 2.26 (3H, s), 2.51 (3H, s), 3.87 (2H, s), 6.71 (1H, s), 7.18 (2H, d, J = 8.2 Hz), 7.27 (3H, dd, J = 9.3, 1.8 Hz).

General procedure for compounds (6a,b)

A mixture of the suitable intermediate **5a,b** (4.50 mmol), K_2CO_3 (9.00 mmol), and ethyl bromoacetate (6.75 mmol) in CH_3CN (10 ml) was refluxed under stirring for 2–4 h. The mixture was then concentrated *in vacuo*, diluted with cold water, and extracted with CH_2Cl_2 (3 × 15 ml). The solvent was evaporated *in vacuo*, and compounds **6a** and **b** were purified by crystallization from ethanol.

Ethyl-2-{3-methyl-5-[4-(methylthio)benzyl]-6-oxopyridazin-1(6*H*)-yl}acetate (6a)

Mp = 129–131°C; crystallization solvent = EtOH; yield = 99.9%. ^{1}H NMR ($CDCl_3$), δ: 1.31 (3H, t, J = 6.8 Hz), 2.24 (3H, s), 2.51 (3H, s), 3.87 (2H, s), 4.27 (2H, q, J = 6.8 Hz), 4.86 (2H, s), 6.68 (1H, s), 7.17 (2H, d, J = 7.3 Hz), 7.25–7.29 (2H, m).

General procedure for compounds (7a,b)

A suspension of the intermediate **6a** and **6b** (4.40 mmol) in 6 N NaOH (10 ml) was stirred at 80°C for 1–2 h. The mixture was first diluted with ice-cold water and then acidified with 6 N HCl. Products **7a** and **7b** were filtered by suction and recrystallized from ethanol.

2-{3-Methyl-5-[4-(methylthio)benzyl]-6-oxopyridazin-1(6*H*)-yl}acetic acid (7a)

Mp = 87–89°C; crystallization solvent = EtOH; yield = 99.9%. ^{1}H NMR ($CDCl_3$), δ 2.25 (3H, s), 2.51 (3H, s), 3.87 (2H, s), 4.91 (2H, s), 6.69 (1H, s), 7.16 (2H, d, J = 7.6 Hz), 7.25 (2H, d, J = 7.6 Hz).

General procedure for compounds (1) [Cilibrizzi et al., 2009] and (8a-c)

To a cooled (–5°C) and stirred solution of the appropriate carboxylic acid **7a,b** (0.90 mmol), in anhydrous tetrahydrofuran (6 ml), Et_3N (3.15 mmol) was added. After 30 min, the mixture was allowed to warm up to 0°C, and ethyl chloroformate (0.99 mmol) was added. After 1 h, the appropriately substituted arylamine (1.80 mmol) was added, and the reaction was carried out at room temperature (rt) for 12 h. The mixture was then concentrated *in vacuo*, diluted with cold water (10–15 ml) and extracted with CH_2Cl_2 (3 × 15 ml). The solvent was evaporated to obtain final compounds **1** and **8a-c**, which were purified by column chromatography using cyclohexane/ethyl acetate 1:1 for compounds **1** and **8a,c** and cyclohexane/ethyl acetate 2:1 for **8b** as eluents.

***N*-(4-Bromophenyl)-2-{3-methyl-5-[4-(methylthio) benzyl]-6-oxo-pyridazin-1(6*H*)-yl}acetamide (8a)**

Mp = 97–99°C; purified by column chromatography (cyclohexane/ethyl acetate 1:1); yield = 10%. ^{1}H NMR ($CDCl_3$) δ 2.30 (3H, s), 2.50 (3H, s), 3.89 (2H, s), 4.94 (2H, s), 6.80 (1H, s), 7.17 (2H, d, J = 8.2 Hz), 7.24 (2H, d, J = 8.2 Hz), 7.39 (4H, dd, J = 2.6, 5.7 Hz), 9.01 (1H, exch br s). MS (ESI) Calcd. for $C_{21}H_{20}BrN_3O_2S$, 458.37. Found: *m/z* 458.17 $[M + H]^+$. *Anal*. Calcd for $C_{21}H_{20}BrN_3O_2S$: C, 55.03; H, 4.40; N, 9.17. Found: C, 54.92; H, 4.39; N, 9.20.

***N*-(4-Iodophenyl)-2-{3-methyl-5-[4-(methylthio) benzyl]-6-oxo-pyridazin-1(6*H*)-yl}acetamide (8b)**

Mp = 68–70°C; purified by column chromatography (cyclohexane/ethyl acetate 2:1); yield = 46%. ^{1}H NMR ($CDCl_3$) δ 2.30 (3H, s), 2.51 (3H, s), 3.89 (2H, s), 4.93 (2H, s), 6.80 (1H, s), 7.18 (2H, s, J = 8.4 Hz), 7.24-7.28 (4H, m), 7.61 (2H, d, J = 8.8 Hz), 8.92 (1H, exch br s). MS (ESI) Calcd. for $C_{21}H_{20}IN_3O_2S$, 505.37. Found: *m/z* 506.11 $[M + H]^+$. *Anal*. Calcd for $C_{21}H_{20}IN_3O_2S$: C, 49.91; H, 3.99; N, 8.31. Found: C, 49.86; H, 4.01; N, 8.34.

2-[5-(3-Methoxybenzyl)-3-methyl-6-oxopyridazin-1 (6*H*)-yl]-*N*-[4-(methylthio)phenyl]acetamide (8c)

Mp = 166–167°C; purified by column chromatography (cyclohexane/ethyl acetate 1:1); yield = 99.9%. ^{1}H NMR ($CDCl_3$), δ 2.28 (3H, s), 2.45 (3H, s), 3.80 (3H, s), 3.89 (2H, s), 4.95 (2H, s), 6.79–6.85 (4H, m), 7.12–7.15 (1H, m), 7.27 (1H, t, J = 7.8 Hz), 7.39 (2H, d, J = 5.0 Hz), 9.13 (1H, exch br s). MS (ESI) Calcd. for $C_{22}H_{23}N_3O_3S$, 409.50. Found: *m/z* 410.11 $[M + H]^+$. *Anal*. Calcd for $C_{22}H_{23}N_3O_3S$: C, 64.53; H, 5.66; N, 10.26. Found: C, 64.66; H, 5.64; N, 10.22.

***N*-(4-Bromophenyl)-2-[5-(3-methoxybenzyl)-3-methyl-6-oxo-pyridazin-1(6*H*)-yl]ethanethioamide (9)**

Compound **9** was obtained by slow addition of Lawesson's reagent (0.28 mmol) to a stirred solution of

compound **1** (0.14 mmol) in toluene (3 ml), and the reaction was carried out at reflux for 3 h. The solvent was removed *in vacuo*, and the mixture was diluted with ice-cold water and extracted with CH_2Cl_2 (3 × 10 ml). The crude product was finally purified by flash column chromatography using cyclohexane/ethyl acetate 1:1 as eluent, to yield **9** as an amorphous solid. Mp = 68–70°C; crystallization solvent = EtOH; yield = 30%. ^{1}H NMR ($CDCl_3$), δ 2.32 (3H, s), 3.81 (3H, s), 3.92 (2H, s), 5.37 (2H, s), 6.81 (1H, s), 6.83-6.87 (3H, m), 7.28 (1H, t, J = 5.0 Hz), 7.48 (2H, d, J = 8.8 Hz), 7.74 (2H, d, J = 8.8 Hz), 11.46 (1H, exch br s). MS (ESI) Calcd. for $C_{21}H_{20}BrN_3O_2S$, 458.37. Found: *m/z* 458.17 $[M + H]^+$, 482.36 $[M + Na]^+$, 378.45 $[M - Br]^+$, 231.17 $[M - C_8H_7BrNS]^+$. *Anal*. Calcd for $C_{21}H_{20}BrN_3O_2S$: C, 55.03; H, 4.40; N, 9.17. Found: C, 55.08; H, 4.39; N, 9.19.

4-(4-Methoxybenzyl)-6-methylpyridazine-3(2*H*)-thione (10)

Lawesson's reagent (0.87 mmol) was slowly added to a stirred solution of intermediate **5c** (0.87 mmol) in toluene (3 ml), and the reaction was carried out at reflux for 2 h. The mixture was cooled and after 1 h stirring in ice-bath, the precipitate was filtered and purified by recrystallization from ethanol. Mp = 191–193°C; crystallization solvent = EtOH; yield = 47%. ^{1}H NMR ($CDCl_3$), δ 2.30 (3H, s), 3.85 (3H, s), 4.11 (2H, s), 6.57 (1H, s), 6.93 (2H, d, J = 8.5 Hz), 7.17 (2H, d, J = 8.5 Hz), 12.12 (1H, exch br s).

N-(4-Bromophenyl)-2-[4-(4-methoxybenzyl)-6-methylpyridazin-3-ylthio]acetamide (11)

A mixture of compound **10** (0.41 mmol), K_2CO_3 (0.82 mmol), and *N*-(4-bromophenyl)-2-chloro acetamide (0.61 mmol) in CH_3CN (4 ml) was refluxed under stirring for 1.5 h. After cooling, the solvent was evaporated, and the mixture was diluted with cold water. The precipitate was filtered and purified by flash chromatography using cyclohexane/ethyl acetate 1:2 as eluent. Mp = 116–118°C; purified by column chromatography (cyclohexane/ethyl acetate 1:2); yield = 96%. ^{1}H NMR ($CDCl_3$), δ 2.62 (3H, s), 3.84 (3H, s), 3.87 (2H, s), 4.08 (2H, s), 6.84 (1H, s), 6.92 (2H, d, J = 8.5 Hz), 7.11 (2H, d, J = 8.5 Hz), 7.38 (2H, d, J = 8.8 Hz), 7.48 (2H, d, J = 8.8 Hz), 10.26 (1H, exch br s). MS (ESI) Calcd. for $C_{21}H_{20}BrN_3O_2S$, 458.37. Found: *m/z* 458.11 $[M + H]^+$. *Anal*. Calcd for $C_{21}H_{20}BrN_3O_2S$: C, 55.03; H, 4.40; N, 9.17. Found: C, 54.81; H, 4.38; N, 9.19.

3-Chloro-4-(4-methoxyphenoxy)-6-phenylpyridazine (13)

A suspension of 3-chloro-6-phenylpyridazin-4-ol **12** (1.31 mmol), 4-methoxyphenylboronic acid (2.62 mmol), copper acetate (1.96 mmol), and Et_3N (2.62 mmol) in CH_2Cl_2 (10 ml) was stirred for 12 h at rt. The copper salts were filtered off, and the organic layer was extracted with 50% aqueous ammonia (3 × 10 ml), washed with water (10 ml), and dried over Na_2SO_4. After removal of the solvent *in vacuo*, the residue was purified by flash column chromatography using cyclohexane/ethyl acetate 1:1 as eluent. Mp = 124–126°C; purified by column chromatography (cyclohexane/ethyl acetate 1:1); yield = 48%. ^{1}H-NMR ($CDCl_3$), δ: 3.86 (3H, s), 6.99 (2H, d, J = 9.2 Hz), 7.45-7.47 (3H, m), 7.61 (2H, d, J = 9.2 Hz), 7.78-7.80 (2H, m), 7.93 (s, 1H).

4-(4-Methoxyphenoxy)-6-phenylpyridazin-3-amine (14)

A solution of compound **13** in saturated ethanolic ammonia was heated in a sealed stainless steel tube at 180°C for 7 h. The mixture was then concentrated *in vacuo*, and the residue was treated with cold diethyl ether to obtain a crude solid that was recovered by suction and recrystallized by ethanol. Mp = 160–162°C; crystallization solvent = EtOH; yield = 99.9%. ^{1}H-NMR (DMSO), δ: 3.79 (3H, s), 6.66 (2H, exch br s), 6.78 (1H, s), 7.01 (2H, d, J = 8.4 Hz), 7.38-7.43 (3H, m), 7.53 (2H, d, J = 8.4 Hz), 7.73 (2H, d, J = 7.2 Hz).

1-(4-Bromophenyl)-3-[4-(4-methoxyphenoxy)-6-phenylpyridazin-3-yl]urea (15a)

To a stirred solution of compound **14** (0.23 mmol) in anhydrous toluene (3 ml), 4-bromophenyl isocyanate (0.26 mmol) was added. The mixture was refluxed for 6 h. After cooling, the solvent was removed under reduced pressure, and the residue was dissolved in CH_2Cl_2 and washed, in turn, with 2 N HCl (3 × 15 ml), 2 N NaOH (3 × 15 ml), and with H_2O (15 ml). The organic layer was dried over Na_2SO_4 and evaporated *in vacuo* to obtain the crude products, which were purified by flash column chromatography using CH_2Cl_2/CH_3OH (gradient 100:0 to 98:2) as eluent. Mp = 267–269°C; purified by column chromatography (CH_2Cl_2/CH_3OH, gradient 100:0 to 98:2); yield = 25%. ^{1}H-NMR ($CDCl_3$), δ: 3.65 (3H, s), 6.82 (4H, d, J = 8.8 Hz), 7.42–7.48 (5H, m), 7.64 (2H, d, J = 8.8 Hz), 7.89–7.92 (2H, m), 8.55 (1H, exch br s), 8.80 (1H, s), 9.42 (1H, exch br s). MS (ESI) Calcd. for $C_{24}H_{19}BrN_4O_3$, 491.34. Found: *m/z* 491.11 $[M + H]^+$. *Anal*. Calcd for $C_{24}H_{19}BrN_4O_3$: C, 58.67; H, 3.90; N, 11.40. Found: C, 58.55; H, 3.89; N, 11.35.

4-Bromo-N-[4-(4-methoxyphenoxy)-6-phenylpyridazin-3-yl]benzamide (15b)

Et_3N (0.025 ml) and 4-bromobenzoyl chloride (0.67 mmol) were added to a cooled (0°C) and stirred

solution of **14** (0.33 mmol) in anhydrous CH_2Cl_2 (4 ml), and the reaction was mantained under stirring at 0°C for 3 h. Additional 4-bromobenzoyl chloride (0.67 mmol) was added, and the mixture was stirred at rt for 24 h. The solid residue was removed by filtration, and the organic layer was washed with 6 N NaOH (3 × 10 ml), 6 N HCl (3 × 10 ml) and, finally, with cold water (2 × 10 ml). Drying with Na_2SO_4 and evaporation of the solvent *in vacuo* resulted in crude compound **15b**, which was purified by flash chromatography using CH_2Cl_2 as eluent. Mp = 203–204°C; purified by column chromatography (CH_2Cl_2); yield = 63%. ^{1}H-NMR ($CDCl_3$), δ: 3.87 (3H, s), 7.02 (2H, d, J = 8.4 Hz), 7.44–7.49 (3H, m), 7.66 (4H, t, J = 8.4 Hz), 7.83 (2H, s. J = 8.4 Hz), 7.91 (2H, dd, J = 6.0, 2.0 Hz), 8.84 (1H, s), 9.52 (1H, exch br s). MS (ESI) Calcd. for $C_{24}H_{18}BrN_3O_3$, 476.32. Found: *m/z* 476.11 $[M + H]^+$. *Anal*. Calcd for $C_{24}H_{18}BrN_3O_3$: C, 60.52; H, 3.81; N, 8.82. Found: C, 60.46; H, 3.82; N, 8.85.

Ethyl 2-[4-(4-methoxyphenoxy)-6-phenylpyridazin-3-ylamino]acetate (16)

A mixture of the intermediate **14** (0.33 mmol), K_2CO_3 (0.66 mmol), and ethyl bromoacetate (1.00 mmol) in CH_3CN (4 ml) was refluxed with stirring for 8 h. The mixture was then concentrated, diluted with cold water, and extracted with CH_2Cl_2 (3 × 15 ml). The organic layer was dried over Na_2SO_4 and evaporated *in vacuo* to obtain the crude product **16**, which was purified by flash chromatography using cyclohexane/ethyl acetate 2:1 as eluent. Mp = 130–132°C; purified by column chromatography (cyclohexane/ethyl acetate 2:1); yield = 79%. ^{1}H NMR ($CDCl_3$), δ: 1.32 (3H, t, J = 7.2 Hz), 3.83 (3H, s), 4.04 (2H, d, J = 5.2 Hz), 4.26 (2H, q, J = 7.2 Hz), 6.39 (1H, s), 6.98 (2H, d, J = 8.8 Hz), 7.39-7.43 (3H, m), 7.62 (2H, d, J = 8.8 Hz), 7.78 (2H, d, J = 7.6 Hz).

2-[4-(4-Methoxyphenoxy)-6-phenylpyridazin-3-ylamino]acetic acid (17)

A suspension of compound **16** (0.30 mmol) in 6 N NaOH (4 ml) was stirred at rt to 80°C for 2 h. The mixture was first diluted with ice-cold water, acidified with 6 N HCl, and then extracted with CH_2Cl_2. The organic layer was dried over Na_2SO_4 and evaporated *in vacuo* to obtain the crude product **17**, which was purified by recrystallization from ethanol. Mp = 203–205°C; crystallization solvent = EtOH; yield = 54%. ^{1}H NMR ($CDCl_3$), δ: 3.83 (3H, s), 3.95 (2H, s), 6.42 (1H, s), 6.94–6.97 (2H, m), 7.40–7.48 (3H, m), 7.57 (2H, d, J = 8.8 Hz), 7.76–7.79 (2H, m).

N-(4-Bromophenyl)-2-[4-(4-methoxyphenoxy)-6-phenylpyridazin-3-ylamino]acetamide (18)

To a cooled (–5°C) and stirred solution of the carboxylic acid **17** (0.14 mmol) in anhydrous tetrahydrofuran (5 ml), Et_3N (0.49 mmol) was added. After 30 min, the mixture was allowed to warm up to 0°C, and ethyl chloroformate (0.15 mmol) was added. After 1 h, 4-bromoaniline (0.28 mmol) was added. The reaction was carried out at room temperature for 5 h. The mixture was then concentrated *in vacuo*, diluted with cold water (10–15 ml), and extracted with CH_2Cl_2 (3 × 15 ml). The solvent was evaporated to obtain final compound **18**, which was purified by column chromatography using cyclohexane/ethyl acetate 1:1 as eluent. Mp = 238–239°C; purified by column chromatography (cyclohexane/ethyl acetate 1:1); yield = 28%. ^{1}H-NMR ($CDCl_3$), δ: 3.83 (3H, s), 4.09 (2H, s), 6.60 (1H, s), 6.96 (2H, d, J = 9.2 Hz), 7.41-7.49 (7H, m), 7.58 (2H, d, J = 9.2 Hz), 7.76 (2H, dd, J = 5.2, 2.8 Hz), 8.25 (1H, exch br s). MS (ESI) Calcd. for $C_{25}H_{21}BrN_4O_3$, 505.36. Found: *m/z* 505.10 $[M + H]^+$. *Anal*. Calcd for $C_{25}H_{21}BrN_4O_3$: C, 59.42; H, 4.19; N, 11.09. Found: C, 59.53; H, 4.17; N, 11.11.

Pharmacology

Cell culture

Human promyelocytic leukemia HL-60 cells stably transfected with FPR1 (HL-60-FPR1), FPR2 (HL-60-FPR2), or FPR3 (HL-60-FPR3) were cultured in RPMI 1640 medium supplemented with 10% heat-inactivated fetal calf serum, 10 mM HEPES, 100 μg/ml streptomycin, 100 U/ml penicillin, and G418 (1 mg/ml), as previously described [Christophe et al., 2002]. Wild-type HL-60 cells were cultured under the same conditions but without G418.

Isolation of human neutrophils

Blood was collected from healthy donors in accordance with a protocol approved by the Institutional Review Board at Montana State University. Neutrophils were purified from the blood using dextran sedimentation, followed by Histopaque 1077 (Sigma Aldrich, St. Louis, MO USA) gradient separation and hypotonic lysis of red blood cells, as previously described [Schepetkin et al., 2007]. Isolated neutrophils were washed twice and resuspended in HBSS without Ca^{2+} and Mg^{2+} (Hank's balanced salt solution [$HBSS^-$]; Mediatech, Inc., Herndon, VA). Neutrophil preparations were routinely >95% pure, as determined by light microscopy, and >98% viable, as determined by trypan blue exclusion.

Ca^{2+} mobilization assay

Changes in intracellular Ca^{2+} were measured with a FlexStation II scanning fluorometer using a FLIPR 3 calcium assay kit (Molecular Devices, Sunnyvale, CA) for human neutrophils and HL-60 cells. All active compounds were evaluated in parent (wild-type) HL-60 cells to verify that agonists are inactive in nontransfected cells (data not shown). Human neutrophils or HL-60 cells, suspended in $HBSS^-$ containing 10 mM HEPES, were loaded with Fluo-4 AM dye (Invitrogen, Eugene, OR) (1.25 μg/ml final concentration) and incubated for 30 min in the dark at 37°C. After dye loading, the cells were washed with $HBSS^-$ containing 10 mM HEPES, resuspended in HBSS containing 10 mM HEPES and Ca^{2+} and Mg^{2+} ($HBSS^+$), and aliquotted into the wells of a flat-bottomed, half-area-well black microtiter plates (2×10^5 cells/well). The compound source plate contained dilutions of test compounds in $HBSS^+$. Changes in fluorescence were monitored ($\lambda_{ex} = 485$ nm, $\lambda_{em} = 538$ nm) every 5 s for 240 s at room temperature after automated addition of compounds. Maximum change in fluorescence, expressed in arbitrary units over baseline, was used to determine agonist response. Responses were normalized to the response induced by 5 nM fMLF (Sigma Chemical Co., St. Louis, MO) for HL-60-FPR1 and neutrophils, or 5 nM Trp-Lys-Tyr-Met-Val-D-Met-NH_2 (WKYMVm) (Calbiochem, San Diego, CA) for HL-60-FPR2 and HL-60-FPR3 cells, which were assigned a value of 100%. Curve fitting (5–6 points) and calculation of EC_{50} were performed by nonlinear regression analysis of the dose–response curves generated using Prism 5 (GraphPad Software, Inc., San Diego, CA).

Chemotaxis assay

Neutrophils were suspended in $HBSS^+$ containing 2% (v/v) fetal bovine serum (FBS) (2×106 cells/ml), and chemotaxis was analyzed in 96-well ChemoTx chemotaxis chambers (Neuroprobe, Gaithersburg, MD), as previously described [Schepetkin et al., 2007]. In brief, lower wells were loaded with 30 μl of $HBSS^+$ containing 2% (v/v) FBS and the indicated concentrations of test compound, DMSO (negative control), and 1 nM fMLE as a positive control. The number of migrated cells was determined by measuring ATP in lysates of transmigrated cells using a luminescence-based assay (CellTiter-Glo; Promega, Madison, WI), and luminescence measurements were converted to absolute cell numbers by comparison of the values with standard curves obtained with known numbers of neutrophils. The results are expressed as percentage of negative control and were calculated as follows: (number of cells migrating in response to test compounds/spontaneous cell migration in response to control medium) × 100. EC_{50} values were determined by nonlinear regression analysis of the dose–response curves generated using Prism 5 software.

Molecular modeling

The FPR1 homology model was created using the crystal structure of bovine rhodopsin, as reported previously [Movitz et al., 2010]. A Protein Data Bank (PDB) file of the homology model was loaded into the Molegro Virtual Docker (MVD) program (MVD 2010.4.2, Molegro ApS, Katrinebjerg, Denmark). The position of the ligand binding site in the model was recently localized by docking studies of different FPR1 agonists [Movitz et al., 2010; Khlebnikov et al., 2012]. Docking search space was defined as a sphere centered at the carbonyl carbon of the Ala residue in the FPR1 peptide agonist Ac-QAWF in its docking pose obtained by Movitz et al. [2010]. The radius of the sphere was adopted to be equal to 11 Å. This search space encompassed the whole Ac-QAWF molecule and included, at least partially, 36 residues of FPR1. Among these, side chains of 23 residues closest to the center of the search space were set flexible during the docking simulation.

For FPR2 homology modeling, the primary amino acid sequence of FPR2 was submitted to the Phyre2 (Protein Homology/analogy Recognition Engine V2.0) protein fold recognition server (Structural Bioinformatics Group, Imperial College, London; http://www.sbg.bio.ic.ac.uk/phyre2) [Kelley and Sternberg, 2009], and the homology model, created using the crystal structure of bovine rhodopsin, was optimized, as described recently [Schepetkin et al., 2013].

Taking into account a lack of structural information about any ligand-receptor complex with FPR2, we tried to locate cavities in the macromolecule obtained by homology modeling in order to identify the search space for docking. Use of the MVD "Detect cavity" module with probe size 1.2 Å gave two cavities with volumes of 241 and 25 $Å^3$ in the region of the binding site. Positions of these two cavities reflect an asymmetric dumb-bell shape of the binding site. Hence, for FPR2, we also chose a spherical search space with a default radius 15 Å centered at the terminus of the larger cavity directed to the smaller one. This sphere embraced two cavities and eight residues reported by Fujita et al. [Fujita et al., 2011]. Side chains of 45 residues closest to the center of the sphere were considered flexible in the docking study.

Before docking, structures of the compounds were preoptimized using HyperChem software (Hypercube, Inc., Gainesville, FL) with MM+ force field and saved in Tripos MOL2 format. The ligand structures

were then imported into the MVD program with the following options enabled: "Create explicit hydrogens," "Assign charges (calculated by MVD)," and "Detect flexible torsions in ligands." Selected molecules were docked into FPR1 and FPR2 using the search spaces indicated above with a rigid receptor structure. Ligand flexibility was accounted for with respect to torsion angles autodetected in MVD. MolDock score functions were used with 0.3 Å grid resolution. The "Internal H-bond" option was activated in the "Ligand evaluation" menu of Docking Wizard. Fifteen docking runs were performed for each molecule with side chain flexibility enabled for the residues mentioned above. The postprocessing options "Energy minimization" and "Optimize H-bonds" were applied after docking.

RESULTS AND DISCUSSION

We synthesized a series of new pyridazin-3(2*H*)-one-based thioderivatives and pyridazine analogs and screened them in order to identify novel molecules able to activate human neutrophils through FPRs. The final compounds were evaluated for their ability to induce intracellular Ca^{2+} flux in HL-60 cells transfected with FPR1, FPR2, or FPR3, as it is possible to estimate FPR binding using this assay system [Prossnitz et al., 1991; Didsbury et al., 1992]. Both EC_{50} values and relative efficacy, compared with the peptide agonists (fMLF and WKYMVm) and previously described pyridazinones **1–3** (Fig. 1 and [Cilibrizzi et al., 2009]), were determined. All compounds were also evaluated in wild-type, nontransfected HL-60 cells to verify response specificity. Moreover, the compounds that showed the best profile were selected to evaluate their chemotactic activity and capacity to mobilize Ca^{2+} in human neutrophils.

Analysis of pyridazinone derivatives containing a methylthio group in the phenyl ring at position C-4 (Table 1) showed that substitution of OCH_3 at this position of the previously published FPR2-specific agonist **2** (Fig. 1 and [Cilibrizzi et al., 2009]) with SCH_3 resulted in compound **8a**, which was inactive for all FPRs. Thus, differences in steric hindrance between oxygen and sulfur appear to result in loss of agonist activity. Surprisingly, the iodine analog, compound **8b**, had agonist activity in the micromolar range for both FPR1 and FPR2. Similarly, substitution of OCH_3 in the *para* position of the phenylacetamide linker of reference compound **3** (Fig. 1 and [Cilibrizzi et al., 2009]) with SCH_3 (compound **8c**) did not change FPR agonist activity, keeping the potency at micromolar levels. These data suggest that it is possible to modify the *para* position of phenylacetamide side chain, resulting in compounds with similar activity. In contrast, transformation of our lead compound **1** (Fig. 1 and [Cilibrizzi et al., 2009]) by substitution of the oxygen atom in the amide bridge

TABLE 1. Functional Activity of New Pyridazin-3(2*H*)-One Thioderivatives 8a-c and 9 in HL-60 Cells Expressing Human FPR1, FPR2, or FPR3, in Comparison with Reference Compounds 1–3*

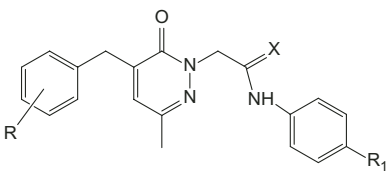

				Ca^{2+} mobilization EC_{50} (μM) and efficacy (%)†		
Compd.	*R*	*X*	R_1	FPR1	FPR2	FPR3
1*	OCH_3 (*m*)	O	Br	3.4 ± 1.6 (75)	3.8 ± 1.5 (70)	N.A.
9	OCH_3 (*m*)	S	Br	N.A.	N.A.	N.A.
2*	OCH_3 (*p*)	O	Br	N.A.	2.4 ± 0.9 (70)	N.A.
8a	SCH_3 (*p*)	O	Br	N.A.	N.A.	N.A.
3*	OCH_3 (*m*)	O	OCH_3	7.7 ± 2.5 (65)	14.4 ± 2.0 (35)	N.A.
8c	OCH_3 (*m*)	O	SCH_3	2.2 ± 0.69 (70)	8.2 ± 2.5 (40)	N.A.
8b	SCH_3 (*p*)	O	I	2.3 ± 0.72 (80)	9.4 ± 2.7 (60)	N.A.
fMLF				0.01	20.4	1.9
WKYMVm				0.5	0.001	0.01

*Values of activity and efficacy are from Cilibrizzi et al. [2009].

†N.A., no activity was observed (no response was observed during first 2 min after addition of compounds under investigation) considering the limits of efficacy >20% and EC_{50} <50 μM. EC_{50} values are presented as the mean ± standard deviation of three independent experiments, in which median effective concentration values (EC_{50}) were determined by nonlinear regression analysis of the dose–response curves (5–6 points) generated using GraphPad Prism 5 with 95% confidential interval ($P < 0.05$). Efficacy (in parentheses) is expressed as % of the response induced by 5 nM fMLF (FPR1) or 5 nM WKYMVm (FPR2 and FPR3).

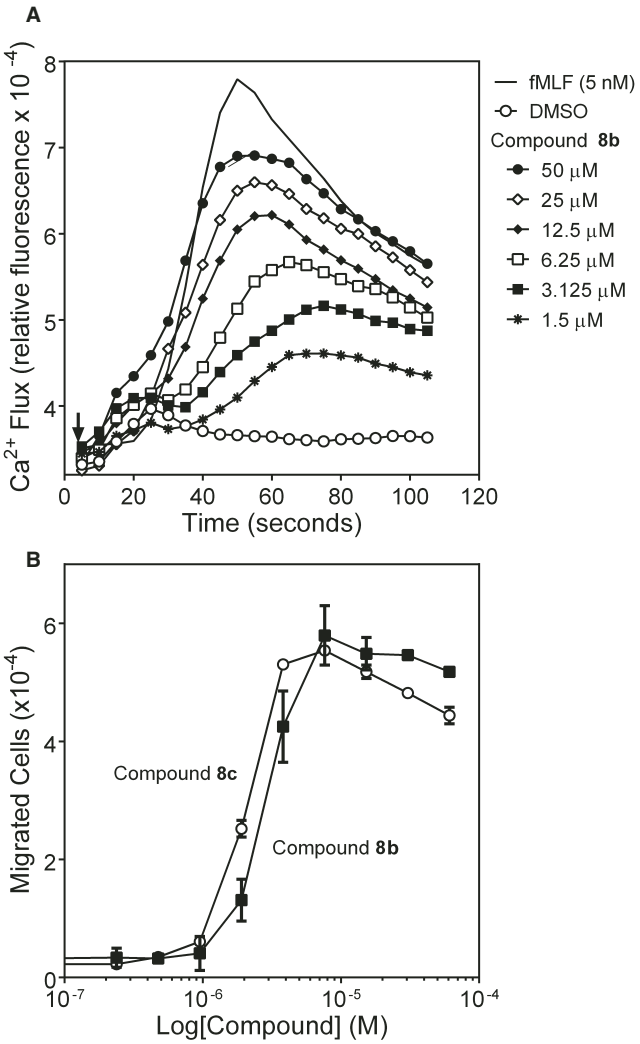

Fig. 4. Activation of human neutrophils by selected compounds. (**A**) Representative kinetics of neutrophil intracellular Ca^{2+} flux after treatment with compound **8b** or fMLF. Human neutrophils were treated with different concentrations of the compound **8b**, 5 nM fMLF, or 1% DMSO (negative control), and Ca^{2+} flux was monitored for the indicated times. The data are from one experiment that is representative of three independent experiments. (**B**) Human neutrophil chemotaxis toward the indicated concentrations of compounds **8b** (■) and **8c** (○) was determined, as described under Materials and Methods. The data are presented as the mean ± standard deviation of duplicate samples from one experiment that is representative of two independent experiments.

with a sulfur atom led to thioamide **9**, which was inactive. Lastly, none of the pyridazine analogs (**11**, **15a**,**b**, and **18**) exhibited FPR agonist activity.

Both FPR1/FPR2 agonists **8b** and **8c** activated human neutrophil Ca^{2+} flux ($EC_{50} = 2.2$ and 2.1 μM, respectively) and chemotaxis ($EC_{50} = 2.9$ and 2.4 μM, respectively). Representative dose–response curves for these activities are shown in Figure 4.

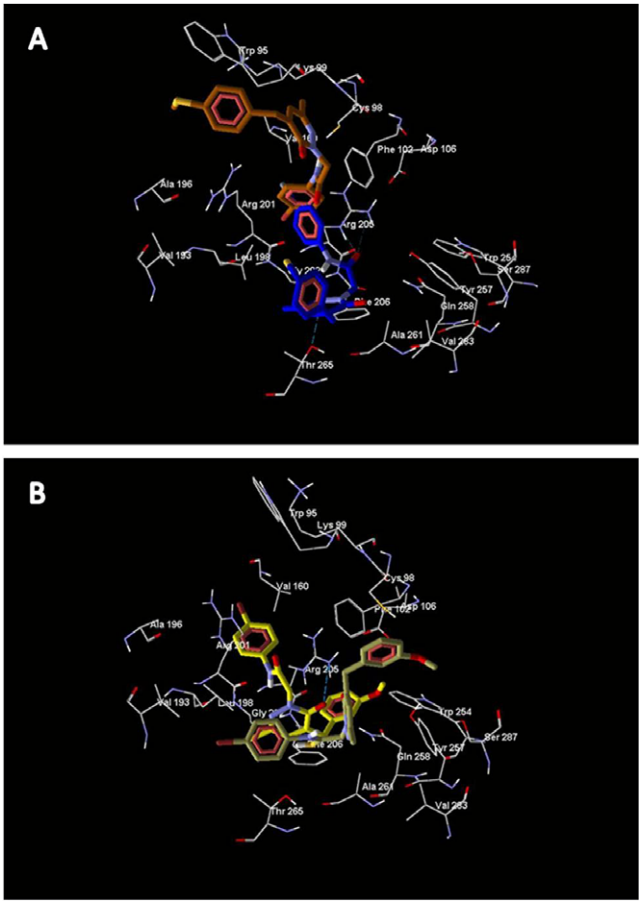

Fig. 5. Docking poses of selected pyridazine derivatives within the FPR1 binding site. (**A**) Poses of active compound **8b** (blue) and inactive compound **8a** (brown). (**B**) Poses of active compound **1** (yellow) and inactive compound **9** (sage). [Color figure can be viewed in the online issue which is available at wileyonlinelibrary.com]

Molecular docking of selected thioderivatives into the FPR1 and FPR2 binding sites was performed to assess how the presence of the sulfur atom might influence the binding modes of the compounds as compared with their oxygen-containing analogs. Taking into account that FPR1 has a more open and broader binding site than FPR2, the docking results were analyzed in terms of partial interactions of ligands with FPR1 residues. As shown in Figure 5, compounds **8a**, **8b**, **1**, and **9** occupy different locations within the receptor. Arg205 is one of the key residues contributing to FPR1 agonist activity [Mills et al., 2000; Khlebnikov et al., 2012], and the highly active peptide fMLE and 2-(benzimidazol-2-ylthio)-N-phenylacetamide-derived FPR1 agonists strongly interacted with Agr205, including formation of H-bonds [Khlebnikov et al., 2012]. Likewise, our docking studies indicated that compound **8b** had interaction energy of –20.02 kcal/mol with Arg205 and was H-bonded to this residue, whereas the

inactive derivative **8a** had a very weak, nonbonded attraction to Arg205. Additionally, molecule **8b** formed H-bonds with Thr265, whereas **8a** was not H-bonded to any FPR1 residue (Fig. 5A). A similar situation occurred for the active and inactive compounds **1** and **9**, respectively (Fig. 5B). Active pyridazine **1** formed an H-bond with Arg205 and had total interaction energy of 32.9 kcal/mol with this residue. On the other hand, compound **9** had a much weaker, nonbonded interaction with Arg205 (–8.82 kcal/mol).

Pairs of sulfur- and oxygen-containing compounds were also compared for their ability to interact with FPR2. As an example, a detailed comparison of docking poses for the active oxygen-containing compound **2** and its inactive methylthio analog **8a** showed that compound **8a** did not have any satisfactory binding mode within the FPR2 binding site and that its best docking pose had significant repulsive interactions with Tyr277 and Ile280 of FPR2. These steric conflicts made it impossible for the sulfur-containing ligand to effectively penetrate into the receptor cavity. In spite of H-bonding with Asn171 and Asp173, this docking pose was energetically unfavorable, and its MolDock score was about 76 kcal/mol higher than that of the active methoxy-derivative **2**. In comparison, the best pose of agonist **2** was well incorporated into the cavity of the 241 $Å^3$ binding site obtained with the MVD "Detect Cavity" feature (see Materials and Methods). The closest nonvalent contact of 2.48 Å occurred between the oxygen atom of the ligand **2** methoxy group and Thr168. An analogous pose would be impossible for compound **8a** whose methylthio group is far more bulky than the methoxy substituent in molecule **2**.

The docking poses of active oxygen-containing derivatives **1–3** and **8c** fit the FPR2 cavity well (Fig. 6A). In contrast, the inactive sulfur-containing pyridazine derivatives **8a** and **9** had molecular fragments outside the cavity, which caused steric hindrances and prevented an effective binding of the ligands with FPR2 (Fig. 6B). Such positions of compounds **8a** and **9** within the binding site were restricted by the bulkiness of sulfur-containing molecular fragments. Hence, these molecules cannot adopt more suitable conformations that are possible for the corresponding oxygen-containing derivatives.

Overall, our docking studies showed that binding modes of oxygen-containing pyridazine derivatives are quite different from their thio-analogs. In the case of FPR2, this is caused mainly by bulkiness of sulfur-containing groups, i.e. by a higher van der Waals radius and longer valence bonds formed by sulfur atoms with respect to oxygen atoms. It is also known that sulfur forms much weaker H-bonds than oxygen [Wood et al., 2008]. Although the importance of H-bonds for binding

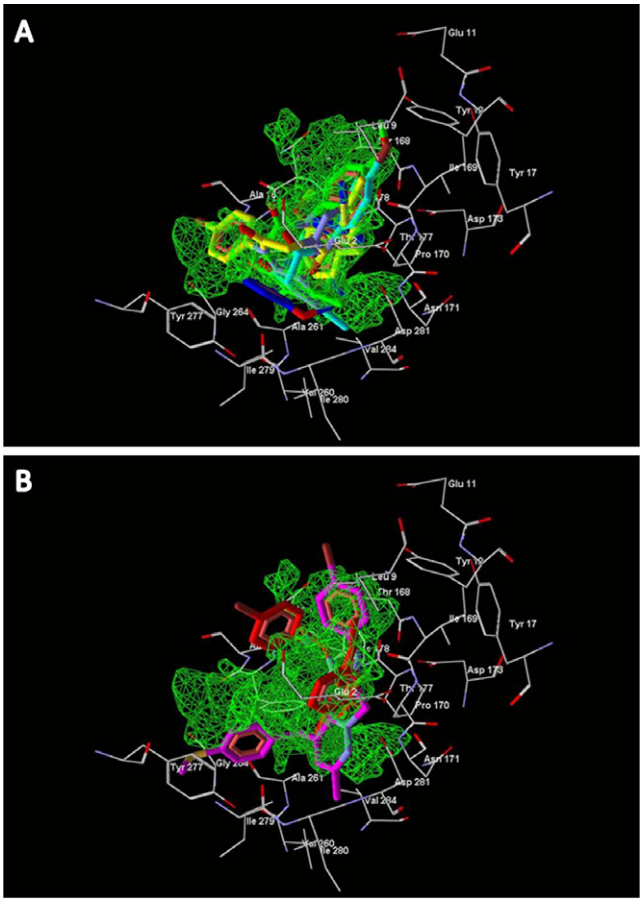

Fig. 6. Docking poses of selected pyridazine derivatives within the FPR2 binding site. The cavity of FPR2 found by the MVD program is shown by a green grid, and residues closest to the cavity are shown. (**A**) Poses of active compounds **1** (yellow), **2** (light-blue), **3** (green), and **8c** (blue) fit the receptor cavity well. (**B**) Poses of inactive compounds **8a** (magenta) and **9** (red) have molecular fragments outside of the cavity (*p*-bromophenyl groups of compounds **8a** and **9**; methyl and methythio groups of compound **8a**). [Color figure can be viewed in the online issue which is available at wileyonlinelibrary.com]

to a receptor was shown here for some active FPR1 and FPR2 agonists, the docking studies indicated that replacement of the sulfur atom by oxygen did not lead to emergence of an H-bond with participation of this oxygen atom in docking. We also confirmed that most active FPR1 agonists strongly interact with Arg205 of the receptor, as described previously [Mills et al., 2000; Khlebnikov et al., 2012].

In conclusion, we synthesized several novel FPR agonists with pyridazinone or pyridazine scaffolds as modified analogs of the previously reported series of FPR agonists [Cilibrizzi et al., 2009]. Among the pyridazinone analogs tested, thioderivatives **8b** and **8c** were mixed FPR1/FPR2 agonists with micromolar activity, whereas all pyridazine analogs and thioderivatives **8a** and **9** were completely inactive. Furthermore,

molecular docking studies suggested that the inactivity of these thioderivatives was due to a weak H-bonding acceptor and bulkiness of sulfur-containing molecular fragments. These findings confirmed the crucial importance of the pyridazinone scaffold for the activity of this class of compounds.

ACKNOWLEDGMENTS

This work was supported in part by National Institutes of Health grant GM103500 and the Montana State University Agricultural Experimental Station.

REFERENCES

Baraldi PG, Preti D, Tabrizi MA, Fruttarolo F, Saponaro G, Baraldi S, Romagnoli R, Moorman AR, Gessi S, Varani K, et al. 2007. N6-[(Hetero)aryl/(cyclo)alkyl-carbamoyl-methoxy-phenyl]-(2-chloro)-5′-N-Ethylcarbox-amido-adenosines: the first example of adenosine-related structures with potent agonist activity at the human A2B adenosine receptor. Bioorg Med Chem 15:2514–2527.

Bokoch GM, Gilman AG. 1984. Inhibition of receptor-mediated release of arachidonic acid by pertussis toxin. Cell 39:301–308.

Bokoch GM, Katada T, Northup JK, Ui M, Gilman AG. 1984. Purification and properties of the inhibitory guanine nucleotide-binding regulatory component of adenylate cyclase. J Biol Chem 259:3560–3567.

Chiang GCH, Olsson T. 2004. Polymer-supported copper complex for C-N and C-O cross-coupling reactions with aryl boronic acids. Org Lett 6:3079–3082.

Christophe T, Karlsson A, Rabiet MJ, Boulay F, Dahlgren C. 2002. Phagocyte activation by Trp-Lys-Tyr-Met-Val-Met, acting through FPRL1/LXA4R, is not affected by lipoxin A4. Scand J Immunol 56:470–476.

Cilibrizzi A, Quinn MT, Kirpotina LN, Schepetkin IA, Holderness J, Ye RD, Rabiet MJ, Biancalani C, Cesari N, Graziano A, et al. 2009. 6-Methyl-2,4-disubstituted pyridazin-3(2*H*)-ones: a novel class of small-molecule agonists for formyl peptide receptors. J Med Chem 52:5044–5057.

Cilibrizzi A, Schepetkin IA, Bartolucci G, Crocetti L, Dal Piaz V, Giovannoni MP, Graziano A, Kirpotina LN, Quinn MT, Vergelli C. 2012. Synthesis, enantioresolution, and activity profile of chiral 6-methyl-2,4-disubstituted pyridazin-3(2H)-ones as potent N-formyl peptide receptor agonists. Bioorg Med Chem 20:3781–3792.

Cui Y, Le Y, Yazawa H, Gong W, Wang JM. 2002. Potential role of the formyl peptide receptor-like 1 (FPRL1) in inflammatory aspects of Alzheimer's disease. J Leukoc Biol 72:628–635.

De Paulis A, Montuori N, Prevete N, Fiorentino I, Rossi FW, Visconte V, Rossi G, Marone G, Ragno P. 2004. Urokinase induces basophil chemotaxis through a urokinase receptor epitope that is an endogenous ligand for formyl peptide receptor-like 1 and -like 2. J Immunol 173:5739–5748.

Didsbury JR, Uhing RJ, Tomhave E, Gerard C, Gerard N, Snyderman R. 1992. Functional high efficiency expression of cloned leukocyte chemoattractant receptor cDNAs. FEBS Lett 297:275–279.

Dufton N, Perretti M. 2010. Therapeutic anti-inflammatory potential of formyl-peptide receptor agonists. Pharmacol Ther 127:175–188.

Edwards BS, Bologa C, Young SM, Balakin KV, Prossnitz ER, Savchuck NP, Sklar LA, Oprea TI. 2005. Integration of virtual screening with high-throughput flow cytometry to identify novel small molecule formylpeptide receptor antagonists. Mol Pharmacol 68:1301–1310.

Fujita H, Kato T, Watanabe N, Takahashi T, Kitagawa S. 2011. Stimulation of human formyl peptide receptors by calpain inhibitors: homology modeling of receptors and ligand docking simulation. Arch Biochem Biophys 516:121–127.

Gierschik P, Sidiropoulos D, Jakobs KH. 1989. Two distinct G_i-proteins mediate formyl peptide receptor signal transduction in human leukemia (HL-60) cells. J Biol Chem 264:21470–21473.

Gilroy DW, Lawrence T, Perretti P, Rossi AG. 2004. Inflammatory resolution: new opportunities for drug discovery. Nat Rev Drug Discov 3:401–416.

Güngör T, Chen Y, Golla R, Ma Z, Corte JR, Northrop JP, Bin B, Dickson JK, Stouch T, Zhou R, et al. 2006. Synthesis and characterization of 3-arylquinazolinone and 3-arylquinazolinethione derivatives as selective estrogen receptor beta modulators. J Med Chem 49:2440–2455.

Jesberger M, Davis TP, Barner L. 2003. Applications of Lawesson's reagent in organic and organometallic syntheses. Synthesis 13:1929–1958.

Kelley LA, Sternberg MJ. 2009. Protein structure prediction on the Web: a case study using the Phyre server. Nat Protoc 4:363–371.

Khlebnikov AI, Schepetkin IA, Kirpotina LN, Brive L, Dahlgren C, Jutila MA, Quinn MT. 2012. Molecular docking of 2-(benzimidazol-2-ylthio)-N-phenylacetamide-derived small-molecule agonists of human formyl peptide receptor 1. J Mol Model 18:2831–2843.

Kilby JM, Hopkins S, Venetta TM, Di Massimo B, Cloud GA, Lee JY, Alldredge L, Hunter E, Lambertm D, Bolognesi D, et al. 1998. Potent suppression of HIV-1 replication in humans by T-20, a peptide inhibitor of gp41-mediated virus entry. Nat Med 4:1302–1307.

Le Y, Murphy PM, Wang JM. 2002. Formyl-peptide receptors revisited. Trends Immunol 23:541–548.

Meng Q, Hesse M. 1990. N-N Bond cleavage: a route to macrocyclic dilactams. Synlett 3:148–150.

Migeotte I, Communi D, Parmentier M. 2006. Formyl peptide receptors: a promiscuous subfamily of G protein-coupled receptors controlling immune responses. Cytok Growth Factor Rev 17:501–519.

Mills JS, Miettinen HM, Jesaitis AJ. 1999. The N-formyl peptide receptor: structure, signaling and disease. In: Serhan CN, Ward PA, editors. Molecular biology of inflammation. Totowa, NJ: Humana Press, p 215–245.

Mills JS, Miettinen HM, Cummings D, Jesaitis AJ. 2000. Characterization of the binding site on the formyl peptide receptor using three receptor mutants and analogs of Met-Leu-Phe and Met-Met-Trp-Leu-Leu. J Biol Chem 275:39012–39017.

Movitz C, Brive L, Hellstrand K, Rabiet MJ, Dahlgren C. 2010. The annexin I sequence gln(9)-ala(10)-trp(11)-phe(12) is a core structure for interaction with the formyl peptide receptor 1. J Biol Chem 285:14338–14345.

Pieretti S, Di Giannuario A, De Felice M, Perretti M, Cirino G. 2004. Stimulus-dependent specificity for annexin 1 inhibition of the inflammatory nociceptive response: the involvement of the receptor for formylated peptides. Pain 109:52–63.

Prossnitz ER, Ye RD. 1997. The N-formyl peptide receptor: a model for the study of chemoattractant receptor structure and function. Pharmacol Ther 74:73–102.

Prossnitz ER, Quehenberger O, Cochrane CG, Ye RD. 1991. Transmembrane signalling by the *N*-formyl peptide receptor in stably transfected fibroblasts. Biochem Biophys Res Commun 179:471–476.

Quach TD, Batey RA. 2003. Gand- and base-free copper (II)-catalyzed C-N bond formation: cross-coupling reactions of organoboron compounds with aliphatic amines and anilines. Org Lett 5:4397–4400.

Quehenberger O, Prossnitz ER, Cavanagh SL, Cochrane CG, Ye RD. 1993. Multiple domains of the N-formyl peptide receptor are required for high-affinity ligand binding. Construction and analysis of chimeric N-formyl peptide receptors. J Biol Chem 268:18167–18175.

Schepetkin IA, Kirpotina LN, Khlebnikov AI, Quinn MT. 2007. High-throughput screening for small-molecule activators of neutrophils: identification of novel *N*-formyl peptide receptor agonists. Mol Pharmacol 71:1061–1074.

Schepetkin IA, Kirpotina LN, Khlebnikov AI, Leopoldo M, Lucente E, Lacivita E, De Giorgio P, Quinn MT. 2013. 3-(1H-indol-3-yl)-2-[3-(4-nitrophenyl)ureido]propanamide enantiomers with human formyl-peptide receptor agonist activity: molecular modeling of chiral recognition by FPR2. Biochem Pharmacol 85:404–416.

Schiffmann E, Showell HV, Corcoran BA, Ward PA, Smith E, Becker EL. 1975. The isolation and partial characterization of neutrophil chemotactic factors from *Escherichia coli*. J Immunol 114:1831–1837.

Serhan CN, Brain SD, Buckley CD, Gilroy DW, Haslett C, O'Neill LA, Perretti M, Rossi AG, Wallace JL. 2007. Resolution of inflammation: state of the art, definitions and terms. FASEB J 21:325–332.

Simon MI, Strathmann MP, Gautam N. 1991. Diversity of G proteins in signal transduction. Science 252:802–808.

Sircar I. 1983. Synthesis of 4-amino-6-phenyl-3(2*H*)-pyridazinones: a general procedure. J Heterocycl Chem 20:1473–1476.

Tsuruky T, Takahata K, Yoshikawa M. 2007. Mechanism of protective effect of intraperitoneally administered agonists for formyl peptide receptors against chemotherapy induced alopecia. Biosci Biothecnol Biochem 71:1198–1202.

Wood PA, Pidcock E, Allen FH. 2008. Interaction geometries and energies of hydrogen bonds to C=O and C=S acceptors: a comparative study. Acta Crystallogr B 64:491–496.

Wrobel J, Millen J, Sredy J, Dietrich A, Kelly JM, Gorham BJ, Sestanj K. 1989. Orally active aldose reductase inhibitors derived from bioisosteric substitutions on tolrestat. J Med Chem 32:2493–2500.

Ye RD, Boulay F, Wang JM, Dahlgren C, Gerard C, Parmentier M, Serhan CN, Murphy PM. 2009. International Union of Basic and Clinical Pharmacology. LXXIII. Nomenclature for the formyl peptide receptor (FPR) family. Pharmacol Rev 61:119–161.

Zhang L, Falla TJ. 2009. Host defense peptides for use as potential therapeutics. Curr Opin Invest Drugs 10:164–171.

Zhou H, Zhou X, Kouadir M, Zhang Z, Yin X, Yang L, Zhao D. 2009. Induction of macrophage migration by neurotoxic prion protein fragment. J Neurosci Methods 181:1–5.